Research paper

EARTHQUAKE SPECTRA

Earthquake Spectra
2020, Vol. 36(1) 322–352

DOI: 10.1177/8755293019878196
journals.sagepub.com/home/eqs
SAGE

Fragility-based methodology for evaluating the time-dependent seismic performance of post-tensioned timber frames

Gabriele Granello[1], Marco Broccardo[2,3], Alessandro Palermo, M.EERI[1], and Stefano Pampanin, M.EERI[4]

Abstract

Since 2010, the construction of post-tensioned wooden buildings (Pres-Lam) has been growing rapidly worldwide. Pres-Lam technology combines unbonded post-tensioning tendons and supplemental damping devices to provide moment capacity to beam–column, wall–foundation, or column–foundation connections. In low seismic areas, designers may choose not to provide additional damping, relying only on the post-tensioning contribution. However, post-tensioning decreases over time due to creep phenomena arising in compressed timber members. As a consequence, there is a reduction of the clamping forces between the elements. This reduction affects the seismic response of Pres-Lam buildings in the case of low- and high-intensity earthquakes. Therefore, understanding and accounting for the post-tensioning losses and their uncertainty are paramount for a robust assessment of the safety of Pres-Lam constructions. So far, however, there have been no comprehensive studies which tackle the overall seismic performance of such systems in the presence of time-varying post-tension losses and the associated uncertainty. This study tackles this research gap by introducing a comprehensive seismic evaluation of Pres-Lam systems based on time-dependent fragility curves. The proposed fragility analysis is specifically designed to account systematically for time-varying post-tension losses and the related uncertainty. The method is applied to two case studies, designed, respectively, with and without supplemental damping devices. In terms of structural performance, results show that the use of additional dissipaters mitigates the effect of post-tensioning loss for earthquakes of high intensity. Conversely, performance under low-intensity earthquakes is strongly dependent on the post-tensioning value, as the

[1]Department of Civil Engineering, University of Canterbury, Christchurch, New Zealand
[2]Swiss Seismological Service, Zurich, Switzerland
[3]Department of Civil Engineering, ETH Zurich, Zurich, Switzerland
[4]Department of Structural and Geotechnical Engineering, Sapienza University of Rome, Rome, Italy

Corresponding author:
Gabriele Granello, Department of Civil Engineering, University of Canterbury, Christchurch 8140, New Zealand.
Email: gabriele.granello@canterbury.ac.nz

reduction of stiffness due to the anticipated rocking motion activation would lead to damage to non-structural elements.

Keywords
Pres-Lam, Post-tensioned timber, Low-damage, Fragility analysis, Seismic performance

Date received: 7 June 2018; accepted: 24 July 2019

Introduction

In the 1990s, the Precast Seismic Structural System (PRESSS) program (Priestley, 1991) showed that the hybrid connection is an efficient low-damage solution for precast concrete walls and frames. The hybrid connection combines unbonded post-tensioning tendons and additional dissipation devices or internal reinforcement. The key idea is to absorb the seismic demand through a rocking mechanism between structural elements.

Specifically, unbonded tendons provide re-centering capabilities to the building, and dissipation devices allow hysteretic energy release as well as additional moment capacity. These damping devices can be placed internally by de-bonding mild steel reinforcement bars (e.g. Curtain et al., 2012) or externally (e.g. Marriott et al., 2009; Sarti et al., 2016) to the connection. In this last case, they have the additional advantage of being easily accessible for replacement.

In 2002, Christopoulos et al. extended the hybrid concept to steel members, supporting the idea that the hybrid connection is material independent. Following this line of thought, in 2005, the technology was extended to engineered timber products (Figure 1), also known as the Pres-Lam system (Palermo et al., 2005).

Extensive laboratory testing (e.g. Moroder et al., 2018; Newcombe et al., 2008; Sarti et al., 2015; Wanninger and Frangi, 2014) showed that the post-tensioned timber connection has remarkable seismic performance: in fact, it presents negligible residual displacements, negligible structural damage in the timber members, and stable non-degrading hysteretic response. Furthermore, analytical and numerical models (e.g. Ponzo et al., 2017; Smith et al., 2014) were developed to capture the dynamic response of such structures.

Following these successful testing, several post-tensioned timber buildings (Figure 2) were built around the world (e.g. Brown et al., 2012; Curtain et al., 2012; Holden et al., 2016; Leyder et al., 2015; Sarti et al., 2017b).

This large body of research has extensively investigated the seismic performance of Pres-Lam structures; however, the long-term performance of such systems is still an open research topic. Post-tensioning decreases over time because of creep phenomena arising in compressed timber members. This causes a reduction of the clamping forces between the structural element and a potential increment of the seismic vulnerability.

Few experimental results are currently available regarding the post-tensioning loss over time expected in a post-tensioned timber system. Davies and Fragiacomo (2011) monitored post-tensioned beam and frame specimens in both controlled and uncontrolled environmental conditions for approximately 12 months. They recorded a post-tensioned loss equal to 9% for the frames, while the post-tensioning loss was found equal to 1.4% for the beams. The reason for such discrepancy was found to be the amount of timber loaded

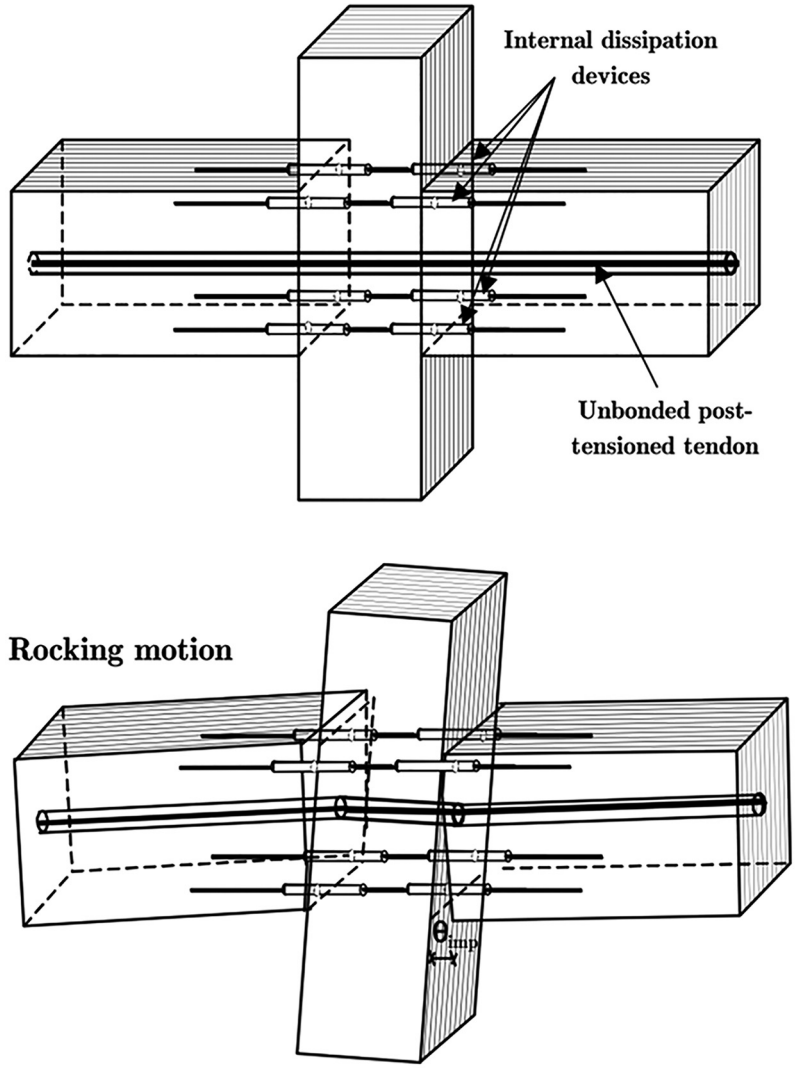

Figure 1. Post-tensioned timber beam–column connection (modified from Palermo et al., 2005).

perpendicular to the grain. The authors also provided analytical creep functions for the New Zealand Laminated Veneer Lumber (LVL) Radiata Pine.

Wanninger et al. (2014) tested post-tensioned Glue Laminated Timber (Glulam) beam–column joints and post-tensioned beams for approximately 18 months. Post-tensioning losses were recorded up to 11% in the joint specimens, while they were recorded equal to 2% in the beams. The authors also provided the analytical creep functions for Swiss ash and spruce Glulam.

Building up on the analytical model proposed by Fragiacomo and Davies (2011), as well as on the experimental creep functions obtained by Davies and Fragiacomo (2011) and Wanninger et al. (2014), a design procedure to estimate the amount of post-tensioning

Figure 2. Examples of operative Pres-Lam structures and beam–column joint detailing (a) Trimble Navigation Offices, Christchurch (courtesy of Paul Drummond) using (b) external steel plates in the beam column joint; (c) ETH House of Natural Resources, Zurich (copyright ETH Zurich-Marco Carocari) using (d) hardwood columns (copyright ETH Zurich-Marco Carocari); (e) Merritt Building, Christchurch (courtesy of Stefano Pampanin) using (f) internal steel plates (courtesy of Stefano Pampanin).

losses in post-tensioned timber systems was proposed by Granello et al. (2018a). This procedure is adopted in this study to describe the mean value of post-tensioning over time.

Since the creep functions were calibrated over 1 or 2 years of experimental data, which is rather a small amount of time compared to a typical building service life, uncertainty is

not negligible in the post-tensioning prediction. Furthermore, creep material properties are subjected to internal variability, and therefore they affect the accuracy of the post-tensioning prediction. Granello et al. (2018b) conducted a preliminary study to evaluate the impact of the variability of post-tensioning loss scenarios on the seismic performance of Pres-Lam frames. Results showed that dissipaters, if provided, are able to mitigate the effect of post-tensioning losses on the interstory drift demand when high seismic events occur. However, being the post-tensioning loss development over time subjected to large uncertainty, a more refined probabilistic approach is necessary to properly estimate the in-time seismic performance of such structures.

Therefore, this study represents the first attempt to develop a holistic strategy for quantifying the lifetime seismic performance of post-tensioned timber structures in the presence of input and post-tension loss uncertainty.

The proposed methodology is based on the well-known concept of fragility analysis (Baker, 2015; Shinozuka et al., 2000); however, in this study, the parameters of the fragility curves are considered as time-varying stochastic processes. This allows a consistent integration of the post-tensioning loss and the related uncertainty.

The structure of this article is as follows. In the first part, both the analytical and probabilistic formulation are presented. Specifically, the first section defines a probabilistic model for estimating the amount of post-tensioning losses in post-tensioned timber systems based on the analytical model proposed by Granello et al. (2018a). The second section focuses on the definition of the time variant fragility functions. The second part of the article focuses on two case studies, specifically, a structure placed in high seismic zone (designed with additional damping devices) and a structure placed in low seismic zone (designed without additional damping devices) to evaluate the influence of additional dissipation devices for the whole range of seismic event scenarios. Ground motion selection and probabilistic modeling of the post-tensioned losses are reported in detail.

Methodology

Probabilistic model for post-tensioning losses in post-tensioned timber systems

Following Granello et al. (2018a), the amount of post-tensioning over time, $\mu_{PT}(t)$, is expressed as:

$$\mu_{PT}(t) = P_0 - \frac{-P_0\left\{\frac{l_{\parallel}\phi_{\parallel}(t)}{E_{\parallel}A_{\parallel}} + \frac{l_{\perp}\phi_{\perp}(t)}{E_{\perp}A_{\perp}} + \frac{lr_p(t)}{E_pA_p\left[1-\chi(t)_p r_p(t)\right]}\right\} + \Delta\epsilon_{\parallel,in}(t)l_{\parallel} + \Delta\epsilon_{\perp,in}(t)l_{\perp} - \Delta\epsilon_{p,in}(t)l}{\frac{l_{\parallel}\left[1+\chi(t)_{\parallel}\phi_{\parallel}(t)\right]}{E_{\parallel}A_{\parallel}} + \frac{l_{\perp}\left[1+\chi(t)_{\perp}\phi_{\perp}(t)\right]}{E_{\perp}A_{\perp}} + \frac{l}{E_pA_p\left[1-\chi(t)_p r_p(t)\right]}} \tag{1}$$

where the indices $\parallel$ and $\perp$ refer to the correspondent timber properties parallel and perpendicular to the grain, respectively. The index, subscript p, instead refers to the post-tensioning steel properties; l, A, and E represent the length of timber under load, the cross-sectional area, and the elastic modulus, respectively; $\phi(t)$ and $r_p(t)$ represent the timber creep function and the steel relaxation function, respectively. The terms $\Delta\epsilon_{in}$ and P_0 represent the inelastic deformation due to changes in environmental conditions and the initial post-tensioning force, respectively. The function $\chi(t)$ takes into account that the analytical

solution is approximated by correcting the creep or relaxation function (Chiorino et al., 1984). The reader specifically interested in the post-tensioning loss calculation is redirected to Granello et al. (2018a) for a comprehensive overview.

In Figure 3, the analytical prediction is reported against the data monitored on an operative post-tensioned timber frame building: Trimble Navigation Building (Granello et al., 2018a). Although the prediction provides a good fit when compared with the data averaged across different frames (Figure 3a), the error (and therefore the uncertainty) with respect to each single frame increases over time (Figure 3b).

To capture the uncertainty evolution, the post-tensioning force, PT,[1] at the $-t$ instant can be expressed as:

$$PT_t = \underbrace{\mu_{PT}(t)}_{mean\ value} + \underbrace{\varepsilon_t}_{uncertainty} \tag{2}$$

where $\mu_{PT}(t)$ is the mean value component, and ε_t is the random variable representing the uncertainty component.

The mean value is defined by Equation 1, and $\varepsilon_t \sim \mathcal{N}(0, \sigma_{PT}(t))$ is assumed normally distributed with zero mean and a time-varying standard deviation (SD), $\sigma_{PT}(t)$. Since the uncertainty in the post-tensioning prediction is increasing exponentially over time (Granello et al., 2018a), $\sigma_{PT}(t)$ is defined as:

$$\sigma_{PT}(t) = c_1 t^{c_2} \tag{3}$$

where c_1, c_2 are the parameters of the model.

Probabilistic formulation of the fragility functions

Fragility curves are defined as the probability of overcoming a specific performance level, conditional to an intensity measure, IM (Baker, 2015; Shinozuka et al., 2000). In earthquake engineering, it is common to assume the lognormal distribution to define the fragility function (Baker, 2015; Porter, 2015) here, reported in Equation 4:

$$P\left(D = d | IM = im;\, \theta_f\right) = \Phi\left(\frac{\ln(im/\alpha)}{\beta}\right) \tag{4}$$

where $\Phi(\cdot)$ is the standard normal cumulative distribution function. The parameters $\theta_f = [\alpha, \beta]$ are, respectively, the median α and the SD β of the fragility function. The quantity IM represents the intensity measure of the seismic excitation, which was selected to be the spectral acceleration. The quantity D represents the performance level, which will be exhaustively discussed in the following section.

Since the performance of post-tensioned structures depend on the amount of post-tensioning, the parameters of the fragility functions are considered dependent on the post-tensioning level PT_t. Specifically, $A_t = \alpha(PT_t)$ and $B_t = \beta(PT_t)$. Since the post-tensioning force is a random variable which depends on the time (i.e. a stochastic process), it follows that also A_t and B_t are time-dependent random variables (i.e. stochastic processes). In the following section, we report the definition of the performance levels, D, while the expressions for A_t and B_t are given for the two case studies in the second part of the article.

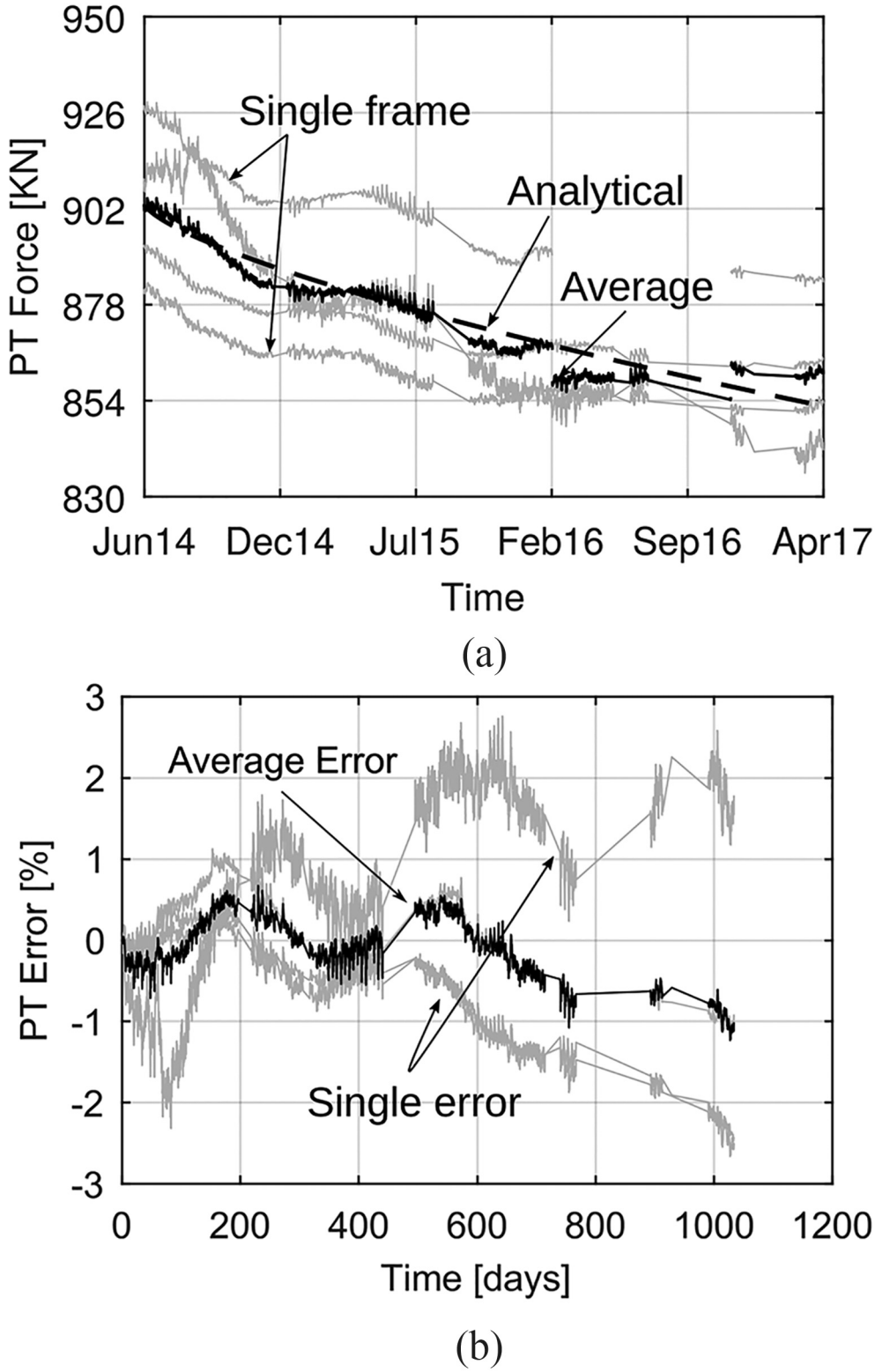

Figure 3. Comparison between analytical post-tensioning force estimation versus experimental data monitored on a post-tensioned timber building: (a) post-tensioning trend and (b) average error.

Performance levels

Following the logic of Federal Emergency Management Agency (FEMA, 2009), the performance of post-tensioned timber structures, D (Equation 4), is defined by specific indicators. In this study, two sets of indicators are used: (1) performance levels in terms of material strain limit and (2) performance levels in terms of interstory drift.

The first set of indicators aims to define suitable performance levels based on the damage of dissipaters and on the stress–strain relationship of timber and steel at the rocking interface. Specifically, five performance levels are defined as follows:

$PL1_{y,ms}$ corresponds to the yielding of the dissipater;
$PL2_{u,ms}$ corresponds to the rupture of the dissipater (i.e. assumed occurring at 6% axial deformation; Priestley, 2000);
$PL3_{y,t}$ corresponds to the yielding of timber in correspondence to the rocking interface;
$PL4_{y,p}$ corresponds to the yielding of the tendon;
$PL5_{u,p}$ corresponds to the rupture of the tendon.

$PL1_{y,ms}$ and $PL2_{u,ms}$ can be classified as serviceability damage state (SLS) because the damage is localized in dissipaters (i.e. it might be necessary to replace them). Conversely, $PL3_{u,t}$ and $PL4_{y,p}$ can be considered as ultimate limit states (ULS) because the structural members are permanently damaged or major repairs are necessary. Finally, $PL5_{u,p}$ is considered as collapse limit state (CLS) because the system fails.

Following the philosophy of most of the building codes (e.g. AS/NZS 1170.5:2004, 2004; Comite Europeen de Normalisation, 2005; FEMA, 2009), the second set of indicators defines performance levels in terms of interstory drift. Such classification assesses the whole building performance rather than focusing on the material strain in critical locations. Specifically, four performance levels are defined as follows:

$PL1_{dr}$ corresponds to the 0.33% of the interstory drift. According to the New Zealand Standard AS/NZS 1170.0:2002 (2002), this is the drift limit for which no damage is expected in the no-structural elements (Figure 4a).
$PL2_{dr}$ corresponds to the 2.5% of the interstory drift. According to the New Zealand Standard AS/NZS 1170.5:2004 (2004), at this level of drift, the main structural elements are subjected to damage, but the whole structure has some capacity left before collapse. It follows that this performance level is defined as a controlled damage limit state (Figure 4b).
$PL3_{dr}$ corresponds to the 6% of the interstory drift. At this drift level, structural collapse is expected (Figure 4c).
$PL4_{dr}$ corresponds to a residual interstory drift post earthquake greater than 0.5%. This performance level is introduced to assess the re-occupancy of the building after the earthquake. In fact, according to several studies (e.g. Hare et al., 2012; McCormick et al., 2008), if the residual drift after the earthquake is greater than 0.5%, the building is likely to be demolished due to uneconomical repairs (Figure 4d).

Given these two sets of indicators, a holistic performance assessment framework for Pres-Lam structures is defined by combining performance levels of the first set with performance levels of the second set as follows:

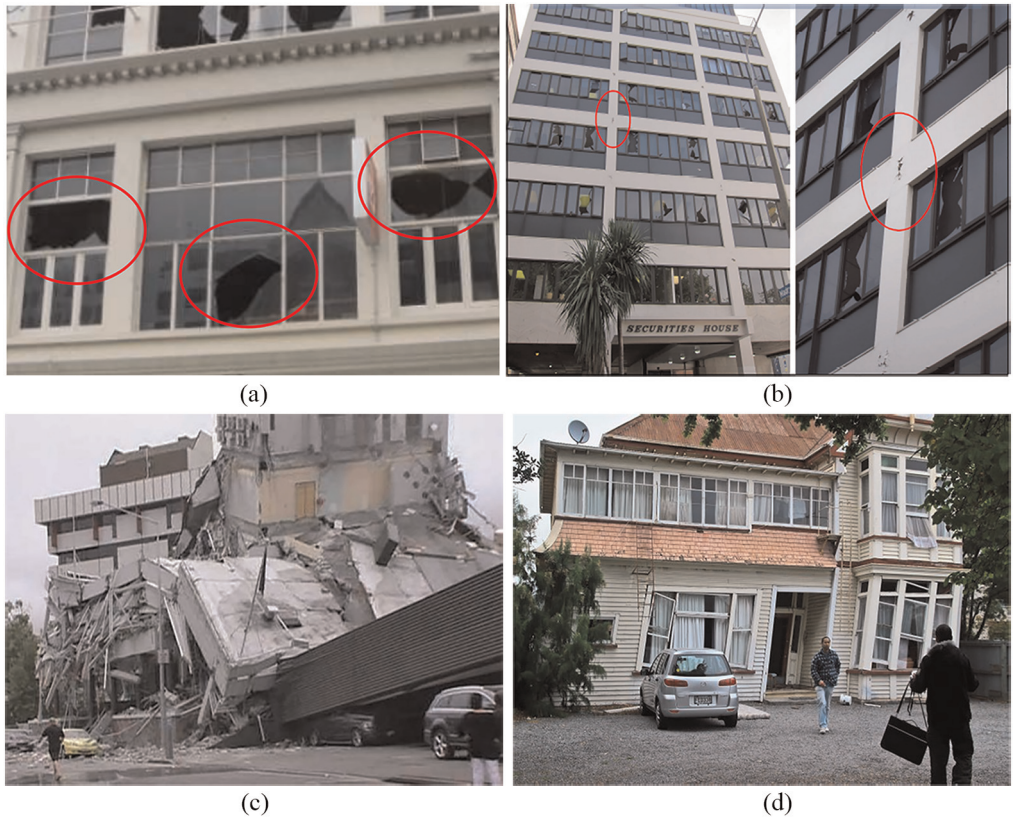

Figure 4. Performance levels: (a) $PL1_{dr}$, expected damage to no-structural elements (courtesy of Stefano Pampanin); (b) $PL2_{dr}$, expected damage to structural elements (courtesy of Stefano Pampanin); (c) $PL3_{dr}$, expected significant damage or collapse (source: www.tvnz.co.nz); (d) $PL4_{dr}$, expected residual deformation after the seismic event (photograph taken by Asher Trafford, https://keithwoodford.wordpress.com/2011/02/27/understanding-the-christchurch-earthquake-building-damage).

1. The serviceability limit state 1 (SLS1) is defined as:

$$PL_{1,a} := PL1_{y,ms} \cup \{0.5\% - 0.7\% \text{ strain deformation}\} \tag{5}$$

Here $PL_{1,a}$ is reached if $PL1_{y,ms}$ occurs, dissipaters are subjected to yielding[2] *or* if the strain deformation is moderate, and within 0.5% to 0.7%.

2. The serviceability limit state 2 (SLS2) is defined as:

$$PL_{1,b} := PL2_{u,ms} \cup PL1_{dr} \tag{6}$$

that is, $PL_{1,b}$ is reached if $PL2_{u,ms}$ *or* $PL1_{dr}$ occurs. In other words, this performance level occurs if the dissipaters have to be replaced at the end of the seismic event (because they are broken), or damage is expected in the non-structural elements.

3. The ULS or controlled damage is defined as:

$$PL_2 := PL3_{y,t} \cup PL2_{dr} \tag{7}$$

that is, PL_2 is reached if $PL3_{y,t}$ *or* $PL2_{dr}$ occurs. In other words, this performance level occurs if damage is expected to occur on the main structural elements or the interstory drift is greater than 2.5%.

4. The CLS is defined as:

$$PL_3 := PL4_{y,p} \cup PL5_{u,p} \cup PL3_{dr} \tag{8}$$

that is, PL_3 is reached if $PL4_{y,p}$ *or* $PL5_{u,p}$ *or* $PL3_{dr}$ occurs. In other words, this performance level occurs if the system fails or excessive interstory drift greater than 5% is observed.

5. The reparability limit state (RLS) is defined as:

$$PL_4 := PL4_{dr} \tag{9}$$

that is, PL_4 is reached if the residual drift after the earthquake is greater than 0.5%. In this case, the building restoration is considered economically unfeasible.

In the following sections, the described methodology is applied to investigate the effect of post-tension losses and associated uncertainty on the seismic performance of two case studies placed in high and low seismic zones, respectively.

Case study buildings

Design

Two case study buildings are designed to be placed in a low (i.e. corresponding to maximum spectral acceleration in correspondence of the plateau equal to $0.54g$ for a 500-year return event) and high (i.e. corresponding to a maximum spectral acceleration in correspondence of the plateau equal to $0.9g$ for a 500-year return event) seismic risk areas, respectively. While the first building is only post-tensioned, the second one is designed with dissipation devices at the beam–column rocking interface. Both structures are designed to be located on type D soil (AS/NZS 1170.5:2004, 2004), corresponding to a deep or soft soil site.

The buildings proposed are a further development of the case study specimen (Figure 5) presented in the New Zealand and Australian Guideline for post-tensioned timber buildings (Pampanin et al., 2013). The structural systems used in that specific case study were Pres-Lam frames in the transverse direction and Pres-Lam walls in the longitudinal direction. This article focuses on the seismic behavior of the frames, which are redesigned to serve as a design case study for this work.

The two four-story case study buildings are designed with a lightweight timber penthouse at the top floor. Each floor is selected to be 32 × 19.5 m in plan with a total floor area of 624 square meters (Figure 5). A building live load of 3 kPa (i.e. office use according to the New Zealand Standard AS/NZS 1170.1:2002, 2002) is assumed to act on a floor system made up of 21 mm thick plywood panels on top of 90 mm × 400 mm timber joists at 0.6 m. To be consistent with the design assumptions reported in the guidelines, no concrete is placed on the top (Pampanin et al., 2013).

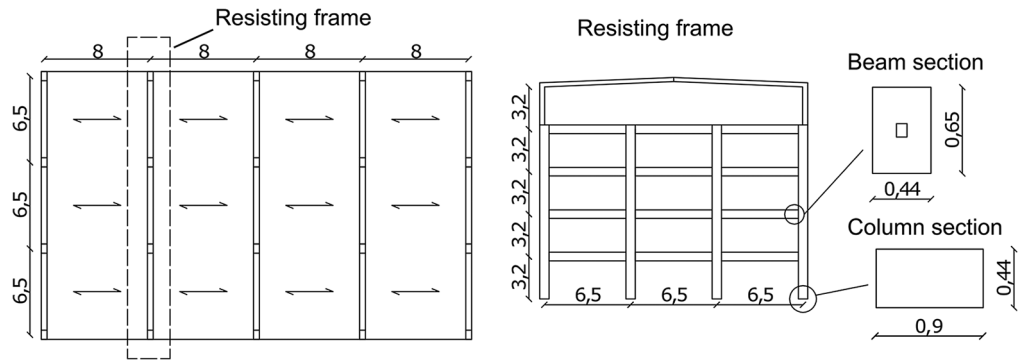

Figure 5. Plan view of the floor, lateral view of the frame, and members' section (note: units are in meters).

Table 1. LVL Grade 16 properties

f_b (MPa)	$f_{c,\,par}$ (MPa)	$f_{c,\,perp}$ (MPa)	f_s (MPa)	E_{par} (GPa)	E_{perp} (GPa)	G (GPa)
65	48	12	4.6	16	0.55	0.8

LVL: Laminated Veneer Lumber.

f_b, bending strength; $f_{c,\,par}$, compression strength parallel to the grain; $f_{c,\,perp}$, compression strength perpendicular to the grain; f_s, shear strength; E_{par}, elastic modulus parallel to the grain; E_{perp}, elastic modulus perpendicular to the grain; G, shear modulus.

The design is carried out by using a displacement-based approach (Priestley et al., 2007). However, the member size and post-tensioning value are governed by the deflection limits to not be exceeded during low-intensity seismic events or excessively strong winds. According to the New Zealand Standard AS/NZS 1170.1:2002 (2002), an interstory drift equal to 0.33% should not be exceeded for an event with a return period equal to 25 years. Therefore, beam and column dimensions of 650 mm × 441 mm, and 900 mm × 441 mm, respectively, are required to meet these criteria.

The timber material used for the design is LVL Radiata Pine Grade 16, properties which according to the manufacturer are reported in Table 1. For the building placed in low seismic hazard, cross-sections with lower dimensions could be designed to optimize the material use. However, in order to compare the results between the two cases, it has been decided to keep the same elements' size.

A summary of the seismic masses (considering the proper combination of dead and live loads according to the New Zealand Standard AS/NZS 1170.5:2004, 2004) is reported in Table 2.

The beam–column connection (detailed in Figure 6), with the addition of the external dissipation devices (Sarti et al., 2016), is designed to target a design re-centering ratio at the ULS, β_{rec} (defined as the ratio between the post-tensioning moment contribution over the total moment capacity), of 0.7. Seven wire strands (properties reported in Table 3) are used as the post-tensioning elements. However, the number of tendons is optimized at each for the two buildings according to the layout reported in Table 4. Ten millimeter external steel plates are designed (see Figures 5b and 6) to protect the timber in the

Table 2. Seismic masses acting on the frame

Floor	Mass (kN)	Mass (kN/frame)	Mass (kN/wall)
4	3130	626	782
3	3193	639	798
2	3193	639	798
1	3193	639	798
Total	12,709	2543	3176

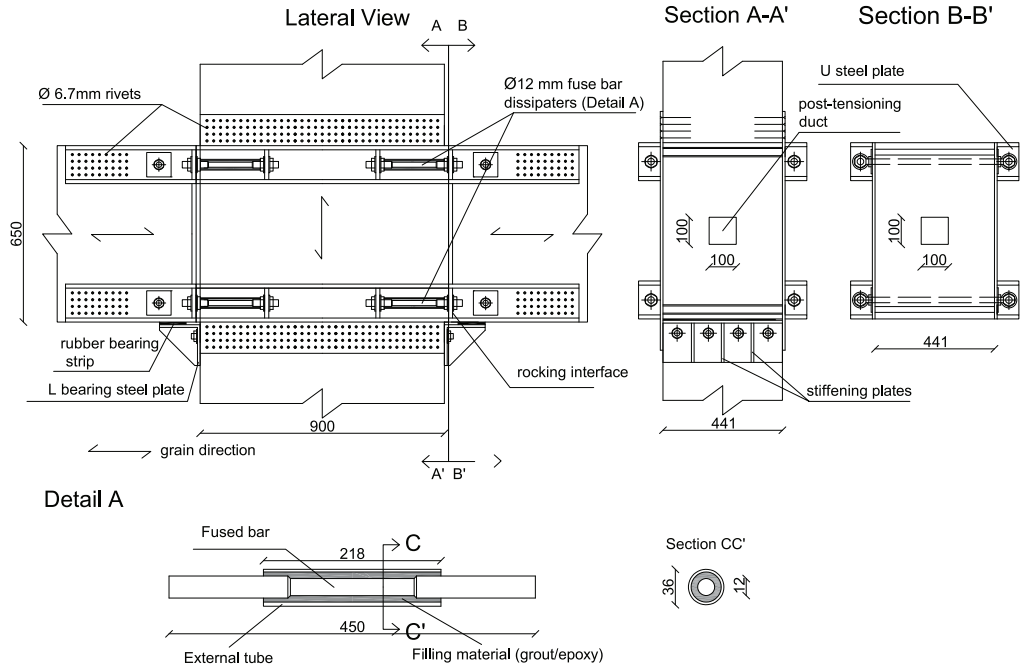

Figure 6. Structural detailing: beam–column hybrid joint and fuse dissipater.

column, which is loaded perpendicular to the grain. This solution, which was adopted in the Trimble Navigation Offices (Brown et al., 2012), also showed to have a beneficial effect in reducing the amount of post-tensioning loss expected (Granello et al., 2018a), as well as providing an anchorage point for the dissipaters.

While post-tensioning tendons are positioned at the section centroid of the beam section, dissipaters are placed ±250 mm from the beam centerline (see Figure 6). The properties of the mild steel, used to fabricate the dissipaters, are reported in Table 5, while the layout of the dissipaters is reported in Table 4.

The differences between the two case study buildings are not limited to the use of dissipaters in one of the two. Specifically, a moment resisting connection (detailed in Figure 7) is designed at the column–foundation level, by introducing internal 14-mm diameter steel bars, for the building placed in high seismic area. Although the elastic period of the two case studies is almost identical, the extra moment capacity provided by the steel bars allows

Table 3. Steel tendon properties

Φ_i (mm)	A_{pi} (mm^2)	f_{ptk} (MPa)	f_{pt01k} (MPa)	E_p (GPa)
12.7	100.1	1860	1674	195

Φ_i, tendon diameter; A_{pi}, tendon area; f_{ptk}, ultimate stress; f_{pt01k}, nominal yielding stress; E_p, elastic modulus.

Table 4. Post-tensioned connection detailing with and without additional damping

	Story	Tendons number	Post-tensioning force (kN)	Tendons stress (%f_{pt01k})	Mild steel dissipaters
With dissipaters	1 and 2	3	300	60	4 Φ 12
	3 and 4	2	200	60	4 Φ 10
Without dissipaters	1 and 2	2	200	60	–
	3 and 4	2	200	60	–

Table 5. Mild steel properties

f_y (MPa)	f_u (MPa)	E_s (MPa)	ϵ_y (−)	r (−)
300	420	200	0.0015	0.008

f_y, yielding stress; f_u, ultimate stress; E_s, elastic modulus; ϵ_y, yielding strain; r, post-yielding stiffness ration.

to increase the stiffness once the rocking motion is activated. This detailing was necessary to the interstory drift within an acceptable value for low-intensity earthquakes.

The connection between timber and steel was obtained by injecting epoxy, and the bars were de-bonded for a total length of 200 mm to distribute the plastic demand. A similar solution with the internal bars was previously adopted for the Carterton Event Centre (Curtain et al., 2012).

The possibility of introducing external dissipaters, which would be easier to replace, was also explored. However, this solution was not feasible due to the high number of connectors necessary between the dissipaters and the column. Shear keys are also provided for transferring shear, and therefore avoiding the internal bars working in dowel action.

Modeling approach

The moment–rotation behavior of a post-tensioned rocking connection was defined using an iterative analytical procedure developed by Pampanin et al. (2001), modified by Palermo (2004), extended to the Pres-Lam system by Newcombe et al. (2008), and further developed by Smith (2014). Such moment–rotation laws are implemented in the literature on lumped plasticity models, using multi-spring elements (Sarti et al., 2017a) or rotational spring elements (Ponzo et al., 2017).

The difference between the two models is the ability of the multi-spring model to capture the increase of axial force in the system due to the beam elongation phenomenon. Given the large inertia of the member, this phenomenon is rather important when looking at the behavior of post-tensioned walls (Sarti et al., 2015). However, in the case of

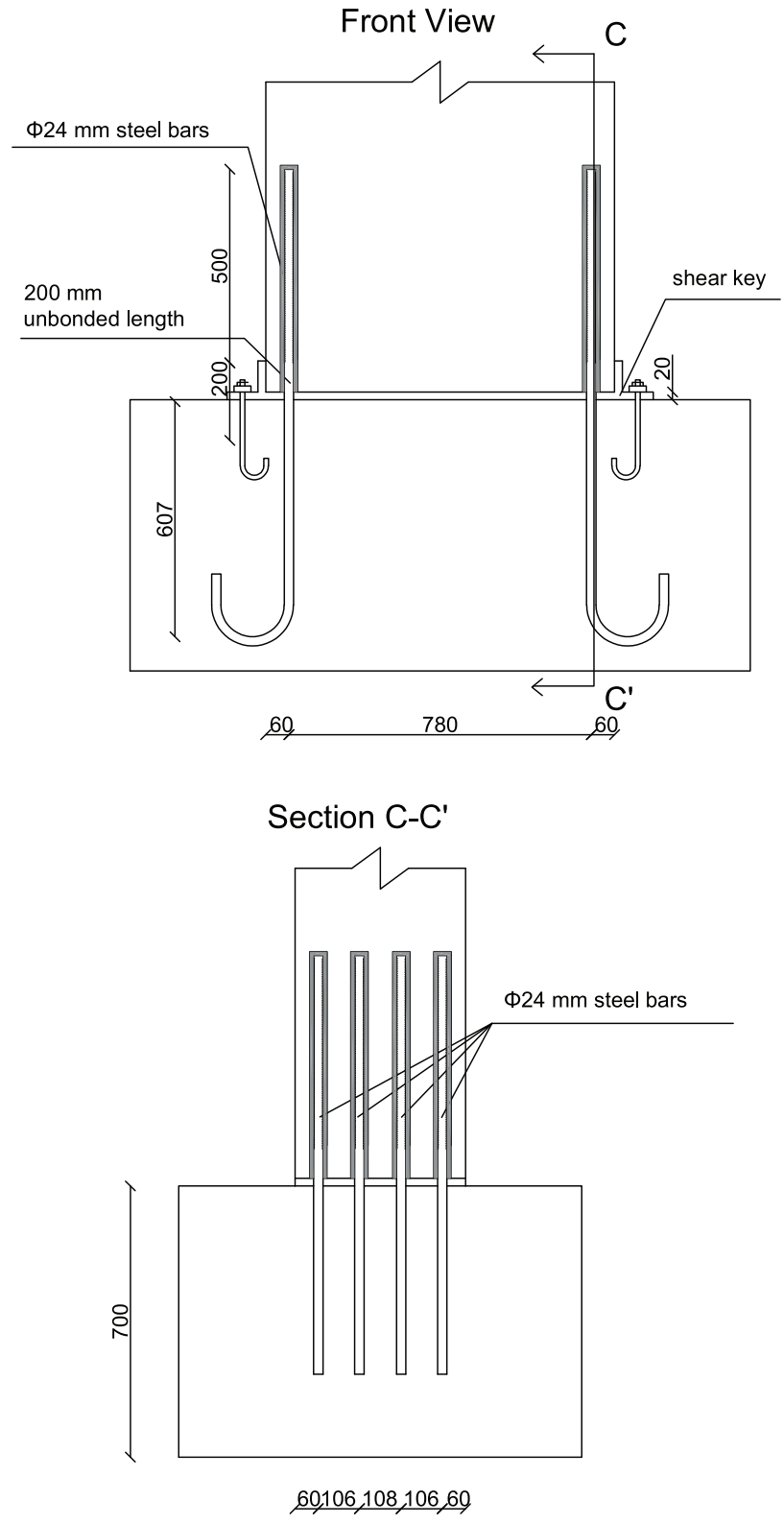

Figure 7. Structural detailing of column–foundation level.

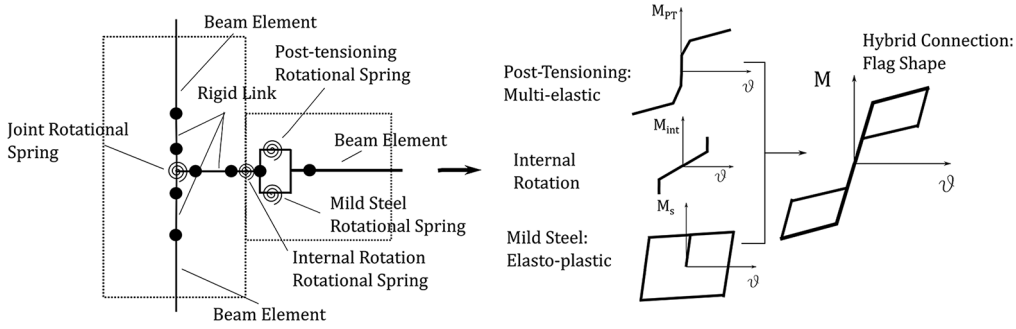

Figure 8. Post-tensioned timber connection modeling.

post-tensioned frames, models based on rotational springs were shown to adequately (up to acceptable errors) predict the behavior of post-tensioned timber specimens when compared to experimental testing (Di Cesare et al., 2017).

In this work, lumped plasticity models (see Figure 8) were calibrated against the moment–rotation response by using rotational springs in parallel and in series, specifically, (1) a multi-linear elastic hysteresis for the post-tensioning contribution, (2) an elasto-plastic rule for the mild steel contribution, and (3) an elastic-rigid rule for the internal rotation before the gap opening contribution. An additional rotational spring was placed at the beam–column joint to take into account the joint shear stiffness, as recommended by Smith (2014). Besides the joints (including the column–foundation one), all the other elements are modeled as elastic members.

Post-tensioning loss estimation

It is assumed that the timber elements are delivered on site with an average moisture content equal to 12%, which is the value commonly provided by the manufacturer. It is also assumed that the environmental temperature at the time of pre-stressing is equal to 10°C. Both these factors affect the post-tensioning trend over time: the moisture content variation affects the creep behavior of timber, while temperature affects the relaxation of steel tendons. For a better understanding of their impact on the post-tensioning loss development, the reader is redirected to Granello et al. (2018a).

The predicted post-tensioning trend over time, $\mu_{PT}(t)$, is reported in Figure 9 and Table 6. It can be noticed that the mean predicted value in 50 years is equal to 16%. The reason for such a "limited" amount, among other factors such as the use of steel plates in the beam–column joint, is because the ratio between the post-tensioning steel area A_p over the timber section $A_{\parallel} = A_{\perp}$ is very low. Such scenario is more likely to happen when designing post-tensioned timber frames in high seismic zones, because the members' size is governed by the interstory drift limit when frequent earthquakes occur.

When the procedure was used to evaluate the amount of post-tensioning loss of the Trimble building, it provided reasonable results considering the average value of the frames (Granello et al., 2018a). However, if the prediction is compared with each single frame, it is subjected to greater uncertainty due to the intrinsic variability of each frame.

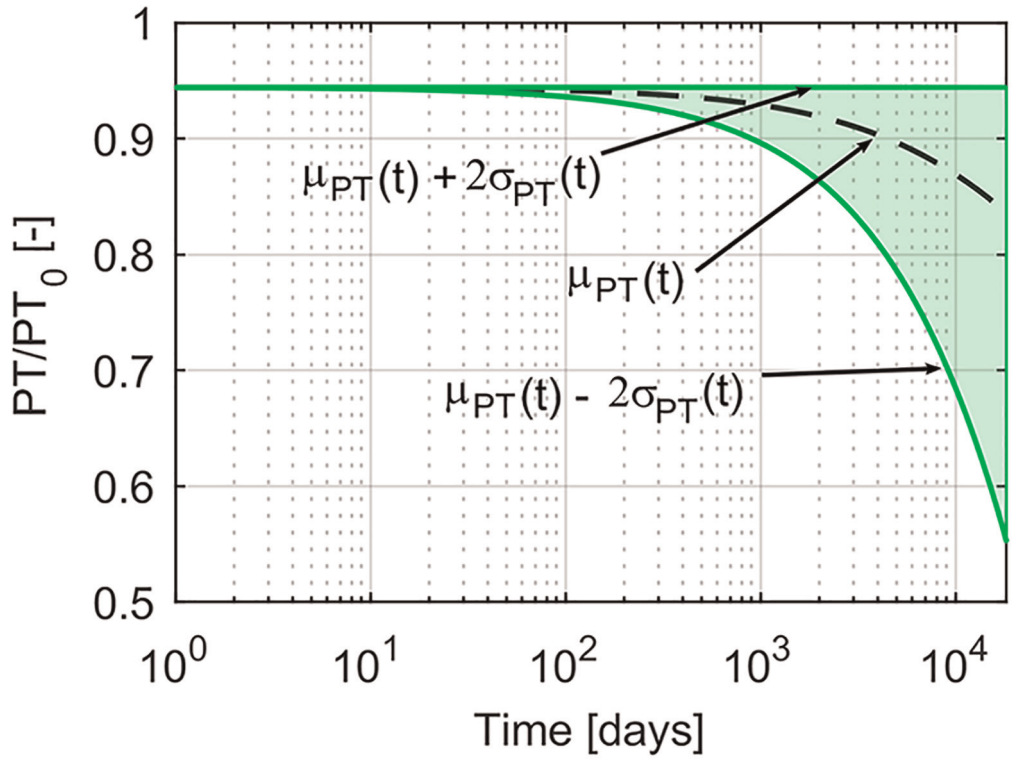

Figure 9. Post-tensioning force over time according to Granello et al. (2018a).
$\mu_{PT}(t)$: average value, $\mu_{PT}(t) + 2\sigma_{PT}(t)$: upper bound, and $\mu_{PT}(t) - 2\sigma_{PT}(t)$: lower bound.

Table 6. Post-tensioning force evolution over time

Post-tensioning	Initial (%)	10 years (%)	25 years (%)	50 years (%)
PT_{avg}	100	91	87	84
PT^{+}_{2STD}	100	94	94	94
PT^{-}_{2STD}	100	82	70	55

$PT_{avg} = \mu_{PT}(t)$: average value, $PT^{+}_{2STD} = \mu_{PT}(t) + 2\sigma_{PT}(t)$: upper bound, and $PT^{-}_{2STD} = \mu_{PT}(t) - 2\sigma_{PT}(t)$: lower bound.

Figure 10 shows the empirical SD of the error between the prediction and experimental results for the Trimble Navigation Offices. It can be observed that the uncertainty on post-tensioning loss is increasing with time, which can be fairly well captured by Equation 3.

In addition to the average losses, Figure 9 and Table 6 report the average value plus (PT^{+}_{2STD}) and minus (PT^{-}_{2STD}) to be two times the SD. Therefore, the green area in Figure 9 represents the possible post-tensioning scenarios within a 95% confidence level, and the average value is represented by the dotted black curve. Note that the initial value is not 100% because of the inelastic deformation of timber and steel at the moment of stressing, which are assumed to occur instantaneously. This value is also considered as the upper boundary of the prediction, which implies a truncated Gaussian distribution for ε_t.

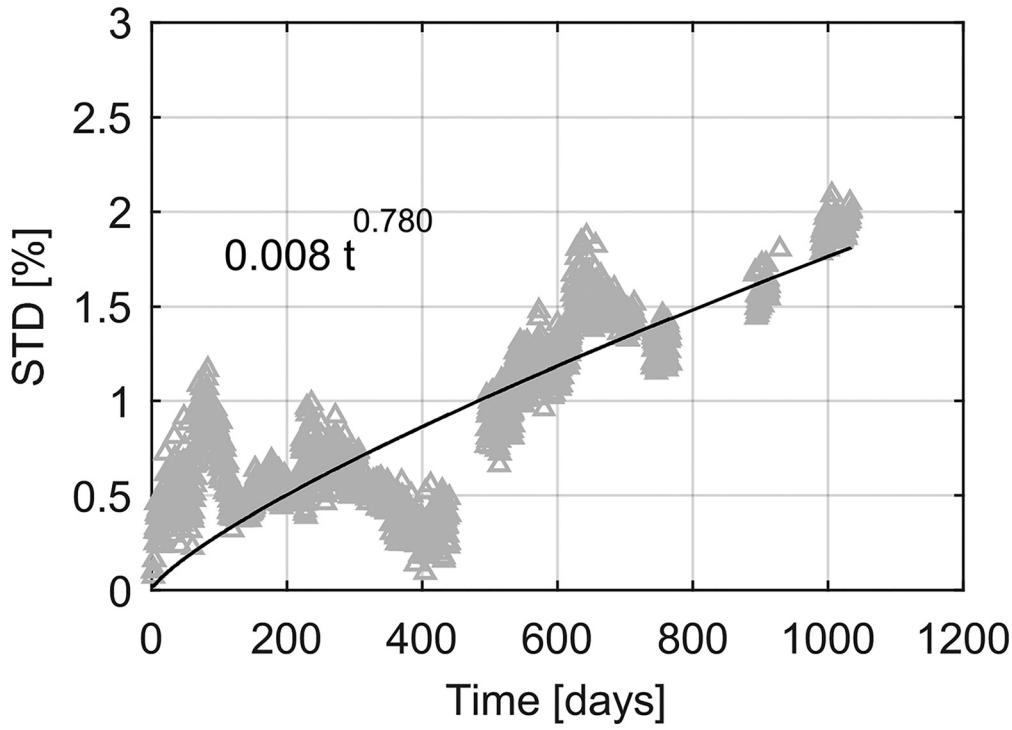

Figure 10. Standard deviation (SD) of the error between the prediction and the data monitored in the Trimble Navigation Offices (Granello et al., 2018a).

Performance levels

Figure 11 reports the moment–rotation response of the beam–column joint of the specimen with dissipaters. Specifically, the response refers to the joints at the first story. The performance levels are also highlighted.

It can be noticed that $PL1_{y,ms}$ occurs almost immediately after the decompression of the joint, for a $\Theta_{gap} = 0.001$. Once the rocking motion is triggered, the dissipaters are activated soon after subjected to yielding.

The dissipaters rupture, that is, $PL2_{u,ms}$ occurs for approximately $\Theta_{gap} = 0.02$; this value can be controlled during the design phase by modifying the unbonded length of the dissipaters. The current practice (Pampanin et al., 2013) suggests designing dissipaters by having an axial deformation equal to 3% at the ULS, which normally targets a 2.5% drift. The building is designed by following this recommendation; therefore, a gap opening equal to $\Theta_{gap} = 0.02$ occurs after reaching 2.5% drift. Once the dissipaters break, their contribution in terms of moment is set equal to 0.

The timber yielding $PL3_{y,t}$, meaning that the most compressed timber fibers exceed the yielding deformation, occurs at approximately $\Theta_{gap} = 0.07$. In this case, the performance level is reached in the beam because the column is protected by steel plates. However, if the column is not adequately protected by using hardwood or steel, this performance level can be reached at lower rotations as the strength of timber perpendicular to the grain is significantly lower than the strength of timber parallel to the grain.

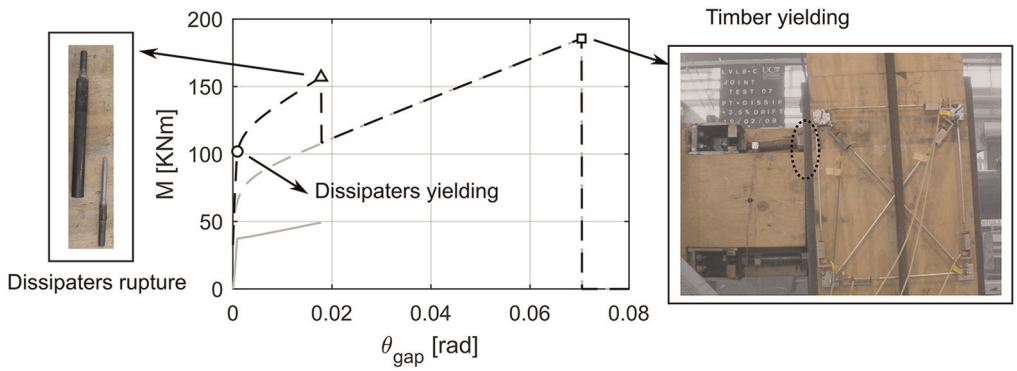

Figure 11. Performance levels for the hybrid rocking connection on the moment–rotation response.

When timber locally yields, the inertia of the entire section is reduced causing a degradation of stiffness. This would imply great rotations, and therefore more fibers would be progressively subjected to yielding. A more refined model, using a more detailed approach, should be used to capture this progressive degradation (Valipour et al., 2016). However, it is conservatively assumed that the moment being carried by the connection, after the yielding of timber, is equal to 0.

The moment–rotation analysis was stopped at $\Theta_{gap} = 0.08$. In fact, given this gap, opening the building would have an interstory drift $\Theta_{interstorey}$ greater than 8%. This happens because $\Theta_{interstorey}$ is the sum of gap opening Θ_{gap} and elastic deformation Θ_{el}:

$$\Theta_{interstorey} = \Theta_{el} + \Theta_{gap} \tag{10}$$

Although the New Zealand building code does not specify a drift limitation in terms of CLS, a limit should be introduced to verify the structure against Maximum Credible Earthquakes (MCEs; Hare et al., 2012). In this study, 6% interstory drift is considered as the CLS.

Because of this assumption, the local performance of the connection has a lack of meaning after 6% interstory drift. Within this limit, the yielding, or even rupture, of tendons is not occurring. Analyses conducted for different connections have shown that the yielding of tendons always occurs at very large interstory drift (greater than 6%). This is due to timber flexibility: because of the great elastic deformation Θ_{el}, the maximum allowable gap opening Θ_{gap} is limited for a given $\Theta_{interstorey}$.

Ground motions selection

The fragility curves were developed by using the multi-stripe method (Baker, 2015). The intensity measure domain was subdivided in "stripes," each one represented by the spectrum given by the New Zealand Standard AS/NZS 1170.5:2004 (2004) for 20, 25, 50, 100, 250, 500, 1000, and 2500 years return period, respectively.

For each spectrum (soil category D) representing the seismic hazard, 80 ground motions were selected for the two sites. The ground motions were extracted from the NGA database (Chiou et al., 2008) and scaled with respect to an anchor point in correspondence of the period, $T^* = 0.85$ s. An example of the spectra and ground motions selected for this study is reported in Figure 12. The spectral values for the different return periods are reported in Table 7.

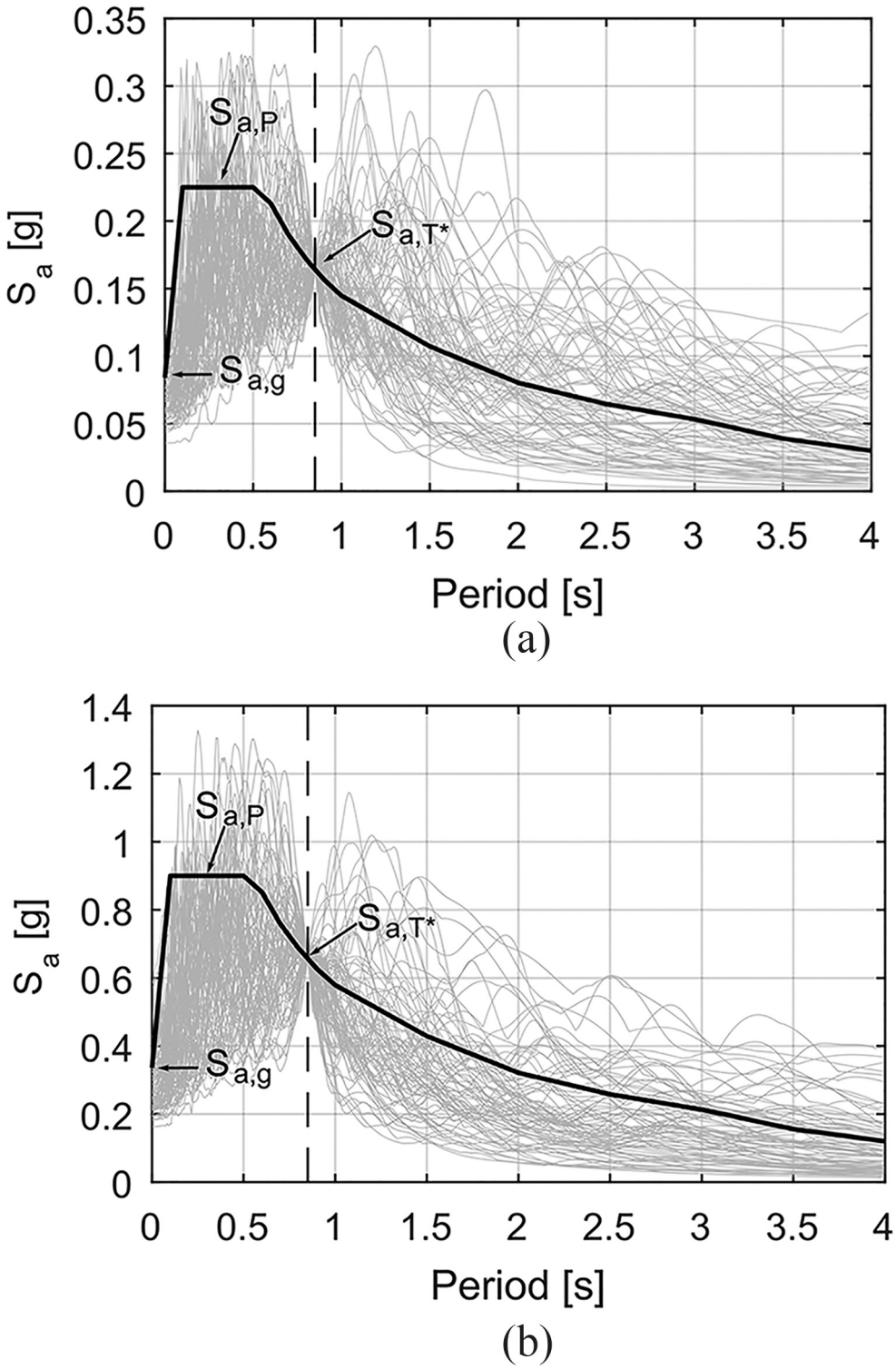

Figure 12. Ground motions spectra for (a) 25 and (b) 500 years return period in high seismic zone. The spectral acceleration in correspondence of ground $S_{a,g}$, plateau $S_{a,P}$, and anchor point $S_{a,T*}$ is highlighted.

Table 7. Spectra acceleration values in correspondence of the ground $S_{a,g}$, in correspondence of the plateau $S_{a,P}$, and in correspondence of the building period S_{a,T^*} for events with different return periods

Return period (years)	Low seismic zone			High seismic zone		
	$S_{a,g}(g)$	$S_{a,P}(g)$	$S_{a,T^*}(g)$	$S_{a,T^*}(g)$	$S_{a,P}(g)$	$S_{a,P}(g)$
20	0.04032	0.1080	0.0752	0.0672	0.1800	0.1254
25	0.0504	0.1350	0.0941	0.0840	0.2250	0.1568
50	0.0706	0.1890	0.1317	0.1176	0.3150	0.2195
100	0.1009	0.2700	0.1881	0.1680	0.4500	0.3135
250	0.1512	0.4050	0.2822	0.2520	0.6750	0.4703
500	0.2016	0.5400	0.3762	0.3360	0.9000	0.6270
1000	0.2621	0.7020	0.4891	0.4368	1.170	0.8151
2500	0.3629	0.9720	0.6772	0.6048	1.620	1.129

The following conditions were considered during the selection process:

1. The ratio between the spectral acceleration of the original ground motion and the code spectrum in correspondence of the first natural period cannot be lower than 0.33 or greater than 3 (New Zealand Standard AS/NZS 1170.5:2004, 2004).
2. The maximum spectral acceleration of the scaled ground motion is not higher than 1.5, which is the maximum spectral acceleration provided by the code.

Both conditions were introduced to avoid

1. having scaling factors too big or too small which dramatically affect the ground motion intrinsic properties (i.e. a ground motion of low intensity does not have the same frequency content of a ground motion of high intensity; Bradley, 2010);
2. adequately representing the hazard in correspondence of the first natural period as well as the plateau range of periods.

Results

Parameters over time

The parameters α and β describing the fragility curves were calculated for 10 levels of post-tensioning loss, that is, 0%, 5%, 10%, 15%, 20%, 25%, 30%, 35%, 40%, and 45%.[3]

In this study, we impose the scaling parameter β for a specific performance level to be constant across the different post-tensioning levels. Imposing a constant β avoids intersection between the fragility curves, which are merely due to "jumps" of β values, due to the classification of engineering demand parameters points on the onset of a limit state threshold.

Therefore, an average beta β_{avg} is estimated for each curve associated with a specific performance level, and the location parameter, α, is recomputed on the reduced parameter space. This corresponds to the engineering assumption that the reliability of the structural system is uniformly decreasing (across all intensity measure values) with the post-tension losses.

The values of β are reported in Figure 13a and b for the building without and with supplemental damping, respectively. The continuous line in both figures shows the average value β_{avg}, which is also reported in Table 8.

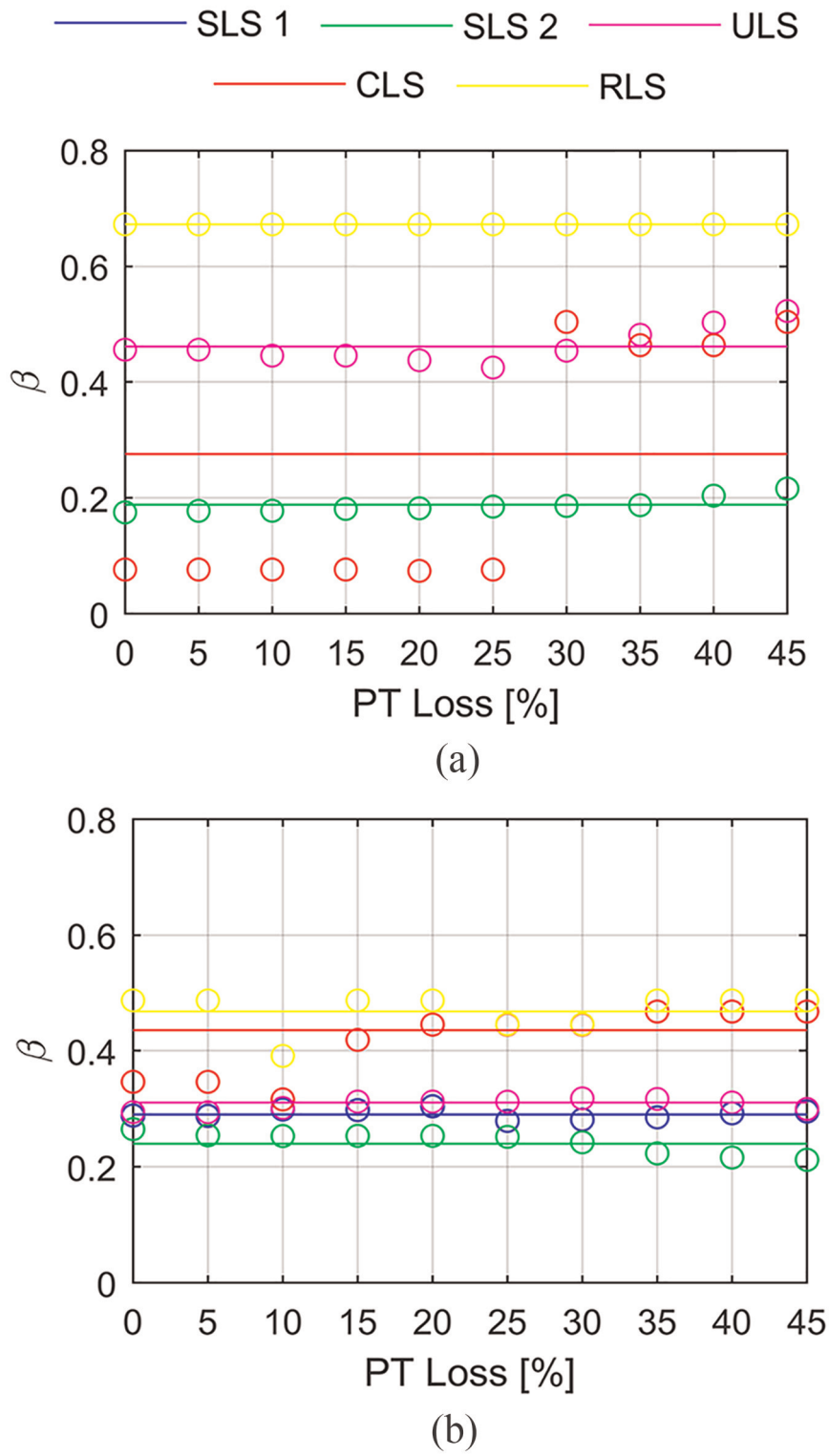

Figure 13. Variance β for the building (a) without and (b) with supplemental damping.

Table 8. Values of β_{avg} and $\alpha = a'x + a_0$, where x is the amount of post-tensioning loss

	Without dissipaters				With dissipaters				
	SLS2	ULS	CLS	RLS	SLS1	SLS2	ULS	CLS	RLS
β_{avg}	0.188	0.461	0.276	0.672	0.290	0.240	0.311	0.436	0.468
a'	–0.00065	–0.0020	–0.0046	–0.55	–0.00041	–0.00015	–0.0013	–0.0031	–0.0012
a_0	0.170	0.896	1.43	60.7	0.133	0.216	1.27	1.95	2.38

SLS2: serviceability limit state 2; SLS1: serviceability limit state 1; ULS: ultimate limit states; CLS: collapse limit state; RLS: reparability limit state.

The values of α are reported in Figure 14 for the two buildings, without and with supplemental damping. Results were interpolated with the following linear model:

$$\alpha(PT) = a'PT + a_0 \tag{11}$$

whose values are reported in Table 8.

It can be noticed from Figure 14 that post-tensioning loss has an impact on the fragility curves. The greater the post-tensioning loss, the lower the value of α. This means that, generally speaking, for a given intensity measure, the probability of overcoming a specific performance level increases while losses increase.

Note that the values of a for the RLS in the building without additional damping are not even present in Figure 14, because out of scale. These values are in fact 10 times greater than the CLS, which means the probability of overcoming re-centering is 10 times lower in average than the probability of reaching 6% drift. This was expected because the building does not have dissipaters, and the re-centering ratio is equal to 1 and does not depend on the post-tensioning level. Also, it has to be noted that the α related to re-centering is higher than the α related to collapse. This means that the probability of re-centering is always higher than the probability of collapse.

By substituting Equation 2 into Equation 11, the expression of α values can be obtained as:

$$A_t = a' \cdot (\mu_{PT}(t) + \varepsilon_t) + a_0 \tag{12}$$

In Figure 15, the values of α for the building without additional damping are reported. The dotted line represents the response over time of the mean, $\mu_{A_t} = a'\mu_{PT}(t) + a_0$, while the boundaries represent the response considering two times the SD $\pm 2\sigma_{A_t}$ dependent on the post-tensioning loss uncertainty. In the same way, the values of A_t for the building with additional dissipaters are reported in Figure 16.

Family of fragility curves

The time variant fragility including the PT uncertainty is given by Equation 15:

$$P\left(D = d | im, \Theta_{f,t} = \theta_f\right) = \Phi\left(\frac{\ln(im/\alpha)}{\beta} | A_t = \alpha, B_t = \beta_{avg}\right) \tag{13}$$

Then, the mean plug-in approximation over time can be obtained as:

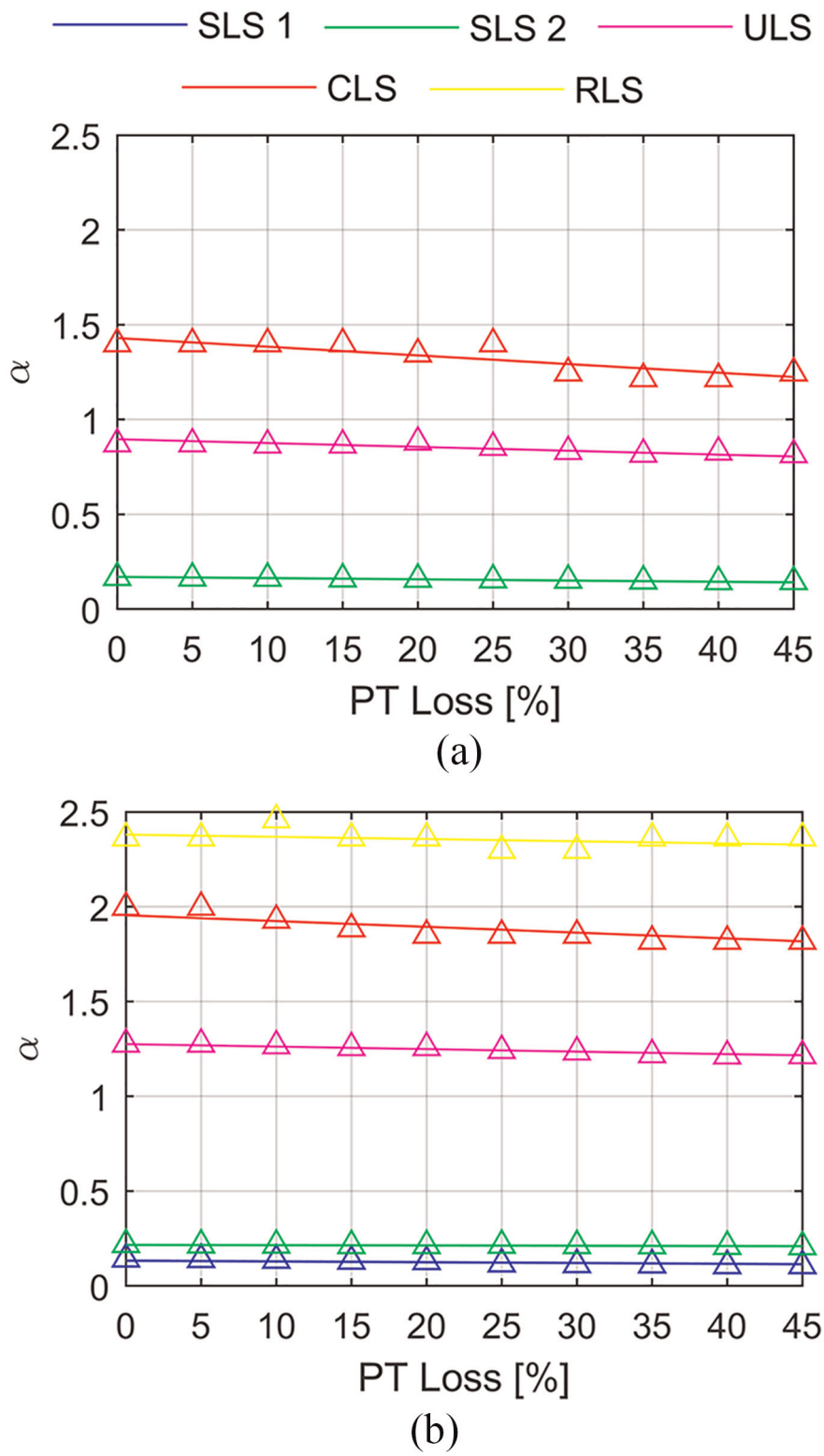

Figure 14. Average α for the building (a) without and (b) with supplemental damping.

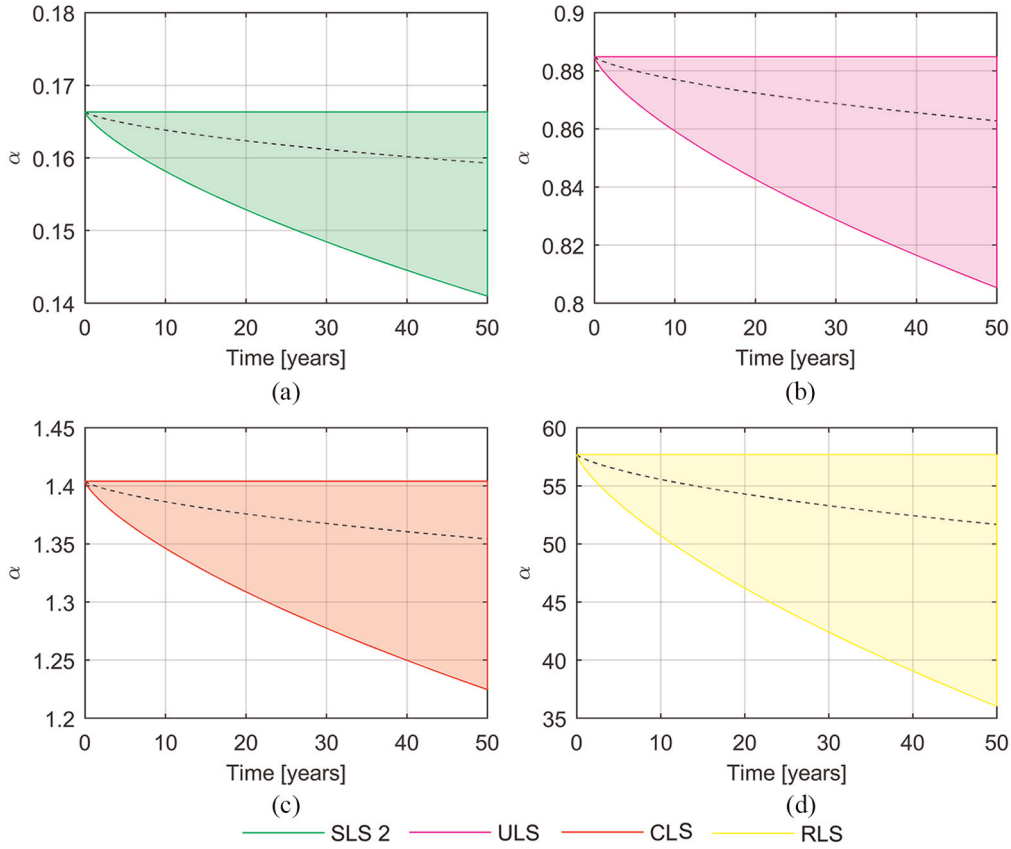

Figure 15. Parameter α over time for each performance level in the building without supplemental damping (black line = mean value μ, boundaries = $\mu \pm 2\sigma$).

$$P\left(D = d | im,\ \Theta_{f,t} = \bar{\theta}_f\right) = \Phi\left(\frac{\ln\left(im/\left(a'\mu_{PT}(t) + a_0\right)\right)}{\beta_{avg}}\right) \tag{14}$$

and the 2-SD plug-in approximation over time can be obtained as:

$$P\left(D = d | im,\ \Theta_{f,t} = \theta_{f,\pm 2\sigma}\right) = \Phi\left(\frac{\ln\left(im/\left(a'\left(\mu_{PT}(t) \pm 2\sigma_{PT}(t)\right) + a_0\right)\right)}{\beta_{avg}}\right) \tag{15}$$

Observe that these fragility functions are *marginal* fragility, that is, they do not include the correlation between different instants of time. It is considered out of the current scope of this study to provide the definition of such time-correlation models mainly because a correlation analysis is not available. Moreover, no inspections or measurements, which will justify updating the model after information becomes available, are included in the design. In this case, a full Gaussian process, which includes a correlation model between different instants of time, can be integrated in the current model. Observe that in this case, the current formulations of A_t and B_t play the role of "prior information."

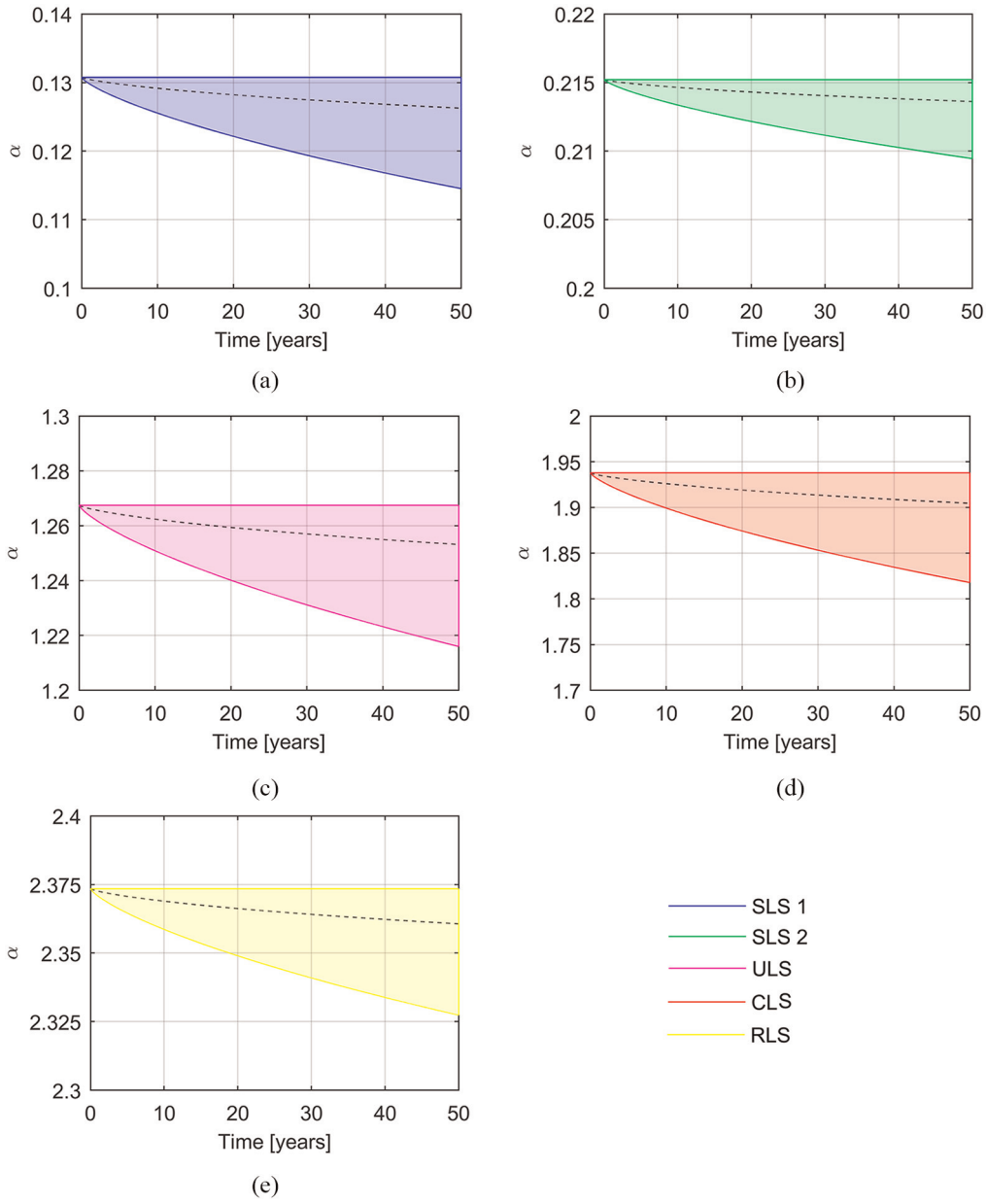

Figure 16. Parameter α over time for each performance level in the building with supplemental damping (black line = mean value μ_{A_t}, boundaries = $\mu_{A_t} \pm 2\sigma_{A_t}$).

Furthermore, if only one fragility is desired (instead of a family of fragility) which also includes the *PT* uncertainty, Equation 16 can be used:

$$P\left(D = d|im,\ \Theta_{f,t} = \theta_f\right) = \int_{\alpha} \Phi\left(\frac{\ln(im/\alpha)}{\beta}|\alpha, \beta_{avg}\right) f(\alpha|t)d\alpha \tag{16}$$

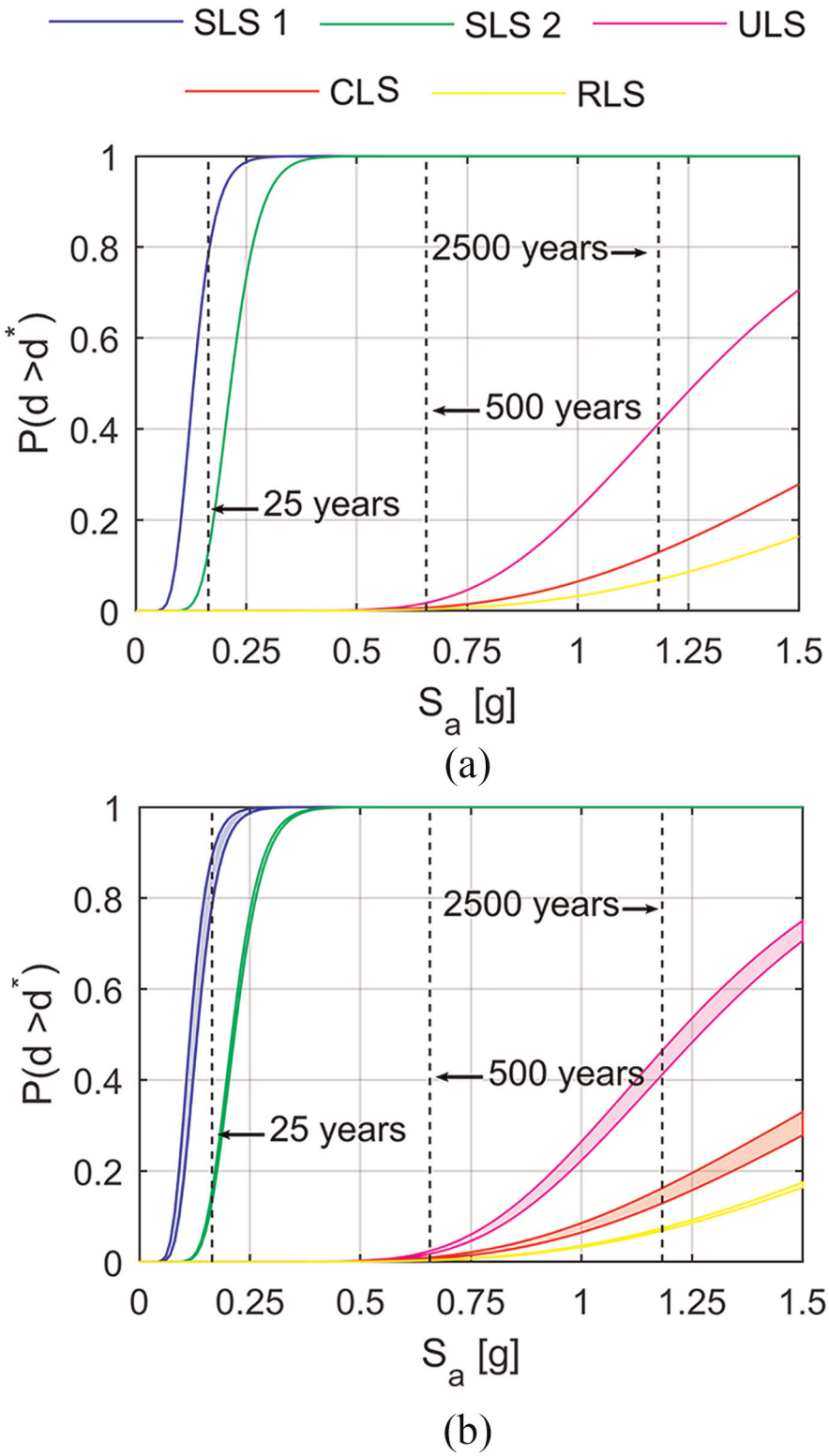

Figure 17. Fragility curves for the building with dissipaters at (a) initial time and (b) after 50 years.

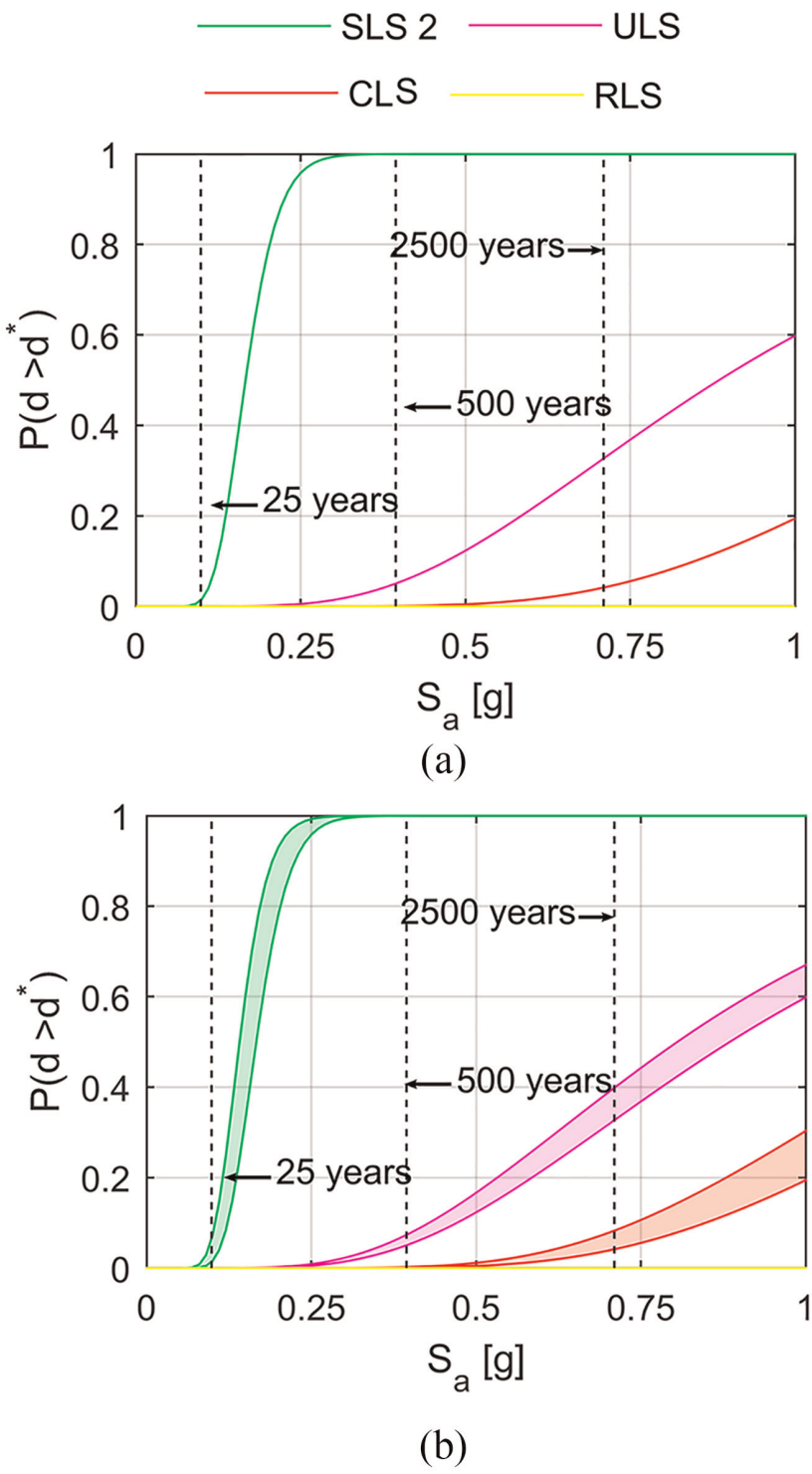

Figure 18. Fragility curves for the building without dissipaters (a) at initial time and (b) after 50 years.

The fragility curves at the initial time for the building with dissipaters are reported in Figure 17a. It can be noticed that the building has less than 20% probability to damage the no-structural elements (SLS2) for a seismic event with a return period equal to 25 years, and a considerably small probability (i.e. 0.01%) to damage to the structural elements (ULS) by an event with return period equal to 500 years. Furthermore, there is less than 16% probability to exceed a 6% drift (CLS) under an event with a return period equal to 2500 years.

In terms of re-centering, the building shows a probability greater than 99.9% to have residual deformation smaller than 0.5% drift for events with a return period lower than 500 years. Furthermore, there is 70% probability that the dissipaters are subjected to yielding for an event with a return period equal to 25 years.

Figure 17b reports the family of fragility curves at 50 years. The lower bound is represented by a scenario with post-tensioning loss equal to 45% (i.e. the expected average value minus 2 SDs). Results show that the performance at SLS2, ULS, CLS, and RLS is similar to the initial one. However, the probability of yielding the dissipaters increases from 70% to almost 100% for an event with a 25-year return period.

Dissipaters are in fact earlier activated when post-tensioning loss occurs, because the clamping force between the beam and the column is reduced. Therefore, they start dissipating energy at lower level of drift. Because of this, the interstory drift does not significantly increase, although the connection capacity is reduced.

However, they are activated more often during the building life, as an event with a lower return period can easily trigger the rocking motion. If dissipaters are external (e.g. in the beam–column joint case), the cost is minor due to the easy access and process. However, if dissipaters are internal (e.g. column–foundation case), the replacement might take more time with a consequently higher cost replacement.

Figure 18a reports the fragility curves for the building without dissipaters at initial time. It can be noticed that the specimen shows approximately 1% probability of damaging the no-structural elements for an event with a 25-year return period; approximately 5% probability of damaging the structural elements for an event with a 500-year return period; and less than 5% probability of overcoming 6% drift for an event with a 2500-year return period. Furthermore, the building shows more than 99.9% probability of having a residual interstory drift lower than 0.5% for all the events with a return period below 2500 years.

Generally speaking, it can be seen from Figure 18b that the area enclosed between the SLS, ULS, and CLS curves at initial time and the same curves at 50 years is greater in respect to the case of the building with additional damping. This means that post-tensioning losses have a greater impact when no dissipaters are provided, and the consequent shift of the fragility curve at 50 years is higher (with respect to the building with additional dissipaters).

When looking at design code provisions, the probability of exceeding the SLS, ULS, and CLS limit state for specific events with a 25-, 500-, and 2500-year return period rises approximately to 7%, 7%, and 8%, respectively. This means that the building still shows an acceptable code compliant behavior after 50 years. However, from the pure seismic performance point of view, the greater shift in the fragility curves over time proves that dissipaters mitigate the effect of post-tensioning loss in terms of overall damage.

In terms of re-centering, the building with no dissipaters after 50 years still maintains a probability of exceeding the RLS lower than 0.1% an event with return period lower than 2500 years. This again is due to the fact that, if dissipaters are not provided, the only post-tensioned joint is able to re-center although losses occur.

Conclusion

The article presented a methodology to evaluate the impact of post-tension losses on the seismic performance of post-tensioned timber frame buildings. The methodology is based on developing a fragility analysis in which parameters are time-dependent to take into account the development and uncertainty of post-tensioning losses.

The post-tensioning force over time was predicted by using an equation from literature, while the uncertainty in the prediction was identified by using data monitored on an operative building. Furthermore, a set of performance levels specifically for post-tensioned timber rocking structures was introduced.

The method was then applied to two Pres-Lam frame buildings, which were designed, respectively, in a high seismic hazard zone (corresponding to a maximum spectral acceleration in correspondence of the plateau equal to $0.9g$ for a 500-year return event) and a low seismic hazard zone (corresponding to maximum spectral acceleration in correspondence of the plateau equal to $0.54g$ for a 500-year return event). The building in the high seismic zone was designed by combining unbonded post-tensioned tendons with dissipaters, while the building in the low seismic zone relies only on unbonded post-tensioned tendons.

In the cases analyzed, results show that post-tensioning losses have minor effects on the seismic performance when looking at the high-magnitude earthquakes. If dissipaters are provided, they further mitigate the effect of post-tensioning losses. However, the reduction of post-tensioning affects the building performance for lower level of earthquakes prematurely activating the rocking motion.

Further building typologies should be investigated to fully understand the influence of post-tensioning loss. However, the fragility-based methodology proposed can be used as a powerful tool for assessing the time-dependent seismic performance of these types of structures.

Declaration of conflicting interests

The author(s) declared no potential conflicts of interest with respect to the research, authorship, and/or publication of this article.

Funding

The author(s) received no financial support for the research, authorship, and/or publication of this article.

Notes

1. Capital letters for PT are used only to indicate the variable "Post Tension," and not to identify a random variable. Conversely, the authors define PT_t as proper random variable defined at time t by Equation 2.
2. In this case, the dissipaters can be replaced after the event at moderate cost (if external), or they can be left installed.
3. The levels were selected based on Figure 9.

References

AS/NZS 1170.0:2002 (2002) *Structural design actions - Part 0: General principles New Zealand standard.*

AS/NZS 1170.1:2002 (2002) *Structural design actions - Part 1: Permanent, imposed and other actions New Zealand Standard.*

NZS 1170.5:2004 (2004) *Structural design actions - Part 5: Earthquake actions - New Zealand*

Baker JW (2015) Efficient analytical fragility function fitting using dynamic structural analysis. *Earthquake Spectra* 31: 579–599.

Bradley BA (2010) A generalized conditional intensity measure approach and holistic ground-motion selection. *Earthquake Engineering & Structural Dynamics* 39: 1321–1342.

Brown A, Lester J, Pampanin S, et al. (2012) Rebuilding timber navigation's offices using a damage-limiting seismic system. In: *Proceedings of the world conference on timber engineering*, Quebec City, QC, Canada, 15–19 July.

Chiorino M, Napoli P, Mola F, et al. (1984) *Structural effects of time-dependent behaviour of concrete*. CEB Bulletin No. 142/142 Bis, Georgi Publishing, Saint-Saphorin.

Chiou B, Darragh R, Gregor N, et al. (2008) NGA project strong-motion database. *Earthquake Spectra* 24: 23–44.

Christopoulos C, Filiatrault A, Uang C, et al. (2002) Posttensioned energy dissipating connections for moment-resisting steel frames. *Journal of Structural Engineering* 128: 1111–1120.

Comite Europeen de Normalisation (2005) *Eurocode 8—Design of Structures for Earthquake Resistance*. Brussels: European Union.

Curtain B, Dekker D, Chung S, et al. (2012) Design of Carterton Event Centre: An example of innovative collaboration between architecture and timber engineering. In: *Proceedings of the 12th world conference on timber engineering (WCTE)*, Auckland, New Zealand, 15–19 July.

Davies M and Fragiacomo M (2011) Long-term behavior of prestressed LVL members—I: Experimental tests. *Journal of Structural Engineering* 137: 1553–1561.

Di Cesare A, Ponzo FC, Nigro D, et al. (2017) Shaking table testing of post-tensioned timber frame building with passive energy dissipation systems. *Bulletin of Earthquake Engineering* 15: 4475–4498.

Federal Emergency Management Agency (FEMA) (2009) *Quantification of building seismic performance factors*. FEMA Report P695, Federal Emergency Management Agency, Washington, DC, June.

Fragiacomo M and Davies M (2011) Long-term behavior of prestressed LVL members—II: Analytical approach. *Journal of Structural Engineering* 137: 1562–1572.

Granello G, Leyder C, Palermo A, et al. (2018a) Design approach to predict post-tensioning losses in post-tensioned timber frames. *Journal of Structural Engineering* 144: 018115.

Granello G, Palermo A, Pampanin S, et al. (2018b) The implications of post-tensioning losses on the seismic response of Pres-Lam frames. *Bulletin of New Zealand Society for Earthquake Engineering* 51: 57–69.

Hare J, Oliver S and Galloway B (2012) Performance objectives for low damage seismic design of buildings. In: *Proceedings of the New Zealand society of earthquake engineering conference*, Christchurch, New Zealand, April 13–15.

Holden T, Devereux C, Haydon S, et al. (2016) NMIT arts & media building: Innovative structural design of a three storey post-tensioned timber building. *Case Studies in Structural Engineering* 6: 76–83.

Leyder C, Wanninger F, Frangi A, et al. (2015) Dynamic response of an innovative hybrid structure in hardwood. *Proceedings of the institution of civil engineers—Construction materials* 168: 132–143.

McCormick J, Aburano H, Ikenaga M, et al. (2008) Permissible residual deformation levels for building structures considering both safety and human elements. In. *Proceedings of the 14th world conference on earthquake engineering*, Beijing, China, 12–17 October.

Marriott D, Pampanin S and Palermo A (2009) Quasi-static and pseudo-dynamic testing of unbonded post-tensioned rocking bridge piers with external replaceable dissipaters. *Earthquake Engineering & Structural Dynamics* 38: 331–354.

Moroder D, Smith T, Dunbar A, et al. (2018) Seismic testing of post-tensioned Pres-Lam core walls using cross laminated timber. *Engineering Structures* 167: 639–654.

Newcombe M, Pampanin S, Buchanan A, et al. (2008) Section analysis and cyclic behavior of post-tensioned jointed ductile connections for multi-story timber buildings. *Journal of Earthquake Engineering* 12: 83–110.

Palermo A (2004) *The use of controlled rocking in the seismic design of bridges*. PhD Thesis, Technical Institute of Milan, Milan.

Palermo A, Pampanin S, Buchanan A, et al. (2005) Seismic design of multi-storey buildings using Laminated Veneer Lumber (LVL). In: *Proceedings of the New Zealand society for earthquake engineering conference*, Wairakei, New Zealand, 11–13 March.

Pampanin S, Palermo A and Buchanan AH (2013) *Design Guide Australia and New Zealand: Post-Tensioned Timber Buildings—EXPAN Design Guides*. Christchurch, New Zealand: Structural Timber Innovation Company.

Pampanin S, Priestley MN and Sritharan S (2001) Analytical modelling of the seismic behaviour of precast concrete frames designed with ductile connections. *Journal of Earthquake Engineering* 5: 329–367.

Ponzo FC, Di Cesare A, Lamarucciola N, et al. (2017) Modelling of post-tensioned timber-framed buildings with seismic rocking mechanism at the column-foundation connections. *International Journal of Computational Methods and Experimental Measurements* 5: 966–978.

Porter K (2015) Beginner's guide to fragility, vulnerability, and risk. In: Beer M, Kougioumtzoglou IA, Patelli E, et al. (eds) *Encyclopedia of Earthquake Engineering*. Heidelberg: Springer, pp. 235–260.

Priestley M (2000) Performance based seismic design. *Bulletin of the New Zealand Society for Earthquake Engineering* 33: 325–346.

Priestley M, Calvi G and Kowalsky M (2007) *Displacement-based Seismic Design of Structures*. Pavia: IUSS Press.

Priestley NMJ (1991) Overview of the PRESSS research program. *PCI Journal* 36: 50–57.

Sarti F, Palermo A and Pampanin S (2015) Quasi-static cyclic testing of two-thirds scale unbonded posttensioned rocking dissipative timber walls. *Journal of Structural Engineering* 142: E4015005.

Sarti F, Palermo A and Pampanin S (2016) Fuse-type external replaceable dissipaters: Experimental program and numerical modeling. *Journal of Structural Engineering* 142: 04016134.

Sarti F, Palermo A, Pam panin S, et al. (2017a) Determination of the seismic performance factors for post tensioned rocking timber wall systems. *Earthquake Engineering & Structural Dynamics* 46: 181–200.

Sarti F, Smith T, Danzig I, et al. (2017b) Pres-Lam in the US: The seismic design of the Peavy Building at Oregon State University. In: *Proceedings of the New Zealand society of structural engineering conference*. Wellington, New Zealand, 27–29 April.

Shinozuka M, Feng MQ, Lee J, et al. (2000) Statistical analysis of fragility curves. *Journal of Engineering Mechanics* 126: 1224–1231.

Smith T (2014) *Post-tensioned timber frames with supplemental damping devices*. PhD Thesis, University of Canterbury, Christchurch, New Zealand.

Smith T, Ponzo FC, Di Cesare A, et al. (2014) Post-tensioned glulam beam-column joints with advanced damping systems: Testing and numerical analysis. *Journal of Earthquake Engineering* 18: 147–167.

Valipour H, Khorsandnia N, Crews K, et al. (2016) Numerical modelling of timber/timber-concrete composite frames with ductile jointed connection. *Advances in Structural Engineering* 19: 299–313.

Wanninger F and Frangi A (2014) Experimental and analytical analysis of a post-tensioned timber connection under gravity loads. *Engineering Structures* 70: 117–129.

Wanninger F, Frangi A and Fragiacomo M (2014) Long-term behavior of posttensioned timber connections. *Journal of Structural Engineering* 141: 04014155.